Structural Optimisation of Web to Sparcap Connection

C. L. Nielsen, C. L. Madsen, F. N. Hjorth, N. K. K. Stagsted, N. M. Bertelsen

Department of Materials and Production, Aalborg University
Fibigerstraede 16, DK-9220 Aalborg East, Denmark
Email: chrnie18, clma18, fhjort18, nstags18, nberte18@student.aau.dk,
Web page: http://www.mechman.mp.aau.dk/

Abstract
This paper aims to optimise the connection between the web and sparcap of an offshore wind turbine blade from Siemens Gamesa Renewable Energy [1]. The objective is to maximise the strength of the connection to increase the overall load bearing capacity of the blade, while maintaining other mechanical properties such as stiffness and mass. This is achieved through change in geometry of the connection with a new connection concept. Static structural finite element analyses are used to evaluate the mechanical properties of the current and new design. The evaluation of strength is achieved by applying maximum-stress and Puck failure criteria on the stress-field of the connection piece and surrounding composite material respectively. Subsequent to a parameterisation, the cross-section of the new design is optimised using Non-linear Programming by Quadratic Lagrangian. Post optimisation analyses are used to further improve, validate and prepare the design for manufacturing. A new design was obtained which can replace the current solution to increase strength for the connection. The stronger design achieved indicates a functional methodology, which can be used by Siemens Gamesa Renewable Energy [1] for developing the connection on larger wind turbine blades.

Keywords: Fibre composite structure, Wind turbine blade, Structural optimisation, Finite element analysis

1 Introduction

The global emissions of CO_2 has led to the seventh of the United Nations sustainable development goals being affordable and clean energy, which includes substantially increasing the share of renewable energy in the global energy mix by 2030 [2]. Increasing the renewable energy produced can be achieved by an increase in the power produced by wind turbines. The amount of wind power available to the wind turbine is controlled by the size of swept area of the wind turbine blades, with a larger size increasing the power available. In order to increase the size of the swept area, longer blades are needed. This requires stronger structural components in the blades, particularly with regards to the flap-wise bending strength. The flap-wise bending strength illustrated in figure 1 and 2, is primarily derived from the web and sparcaps which requires a stronger connection, since the connection is critical to maintain the functionality of the web and sparcaps [1][3].

The sparcap carries most of the bending moment, and the web ensures the distance between the sparcaps, while carrying the shear loads. The sparcap is made of glass-fibre reinforced polymer [GFRP] and carbon-fibre reinforced polymer [CFRP]. The web is made of wood and GFRP in a sandwich structure. The flap-wise bending is caused by a distributed load across the blade, as illustrated in figure 2. The connection piece which is made of polyethylene terephthalate [PET], is used to control the rounding of the GFRP, and increase the strength of the connection illustrated in figure 3. The current connection was developed with the use of sub-component testing and modelling.

Simplified representations of the connection is used in full blade models, with the web directly connected to the sparcap without a connection piece [1].

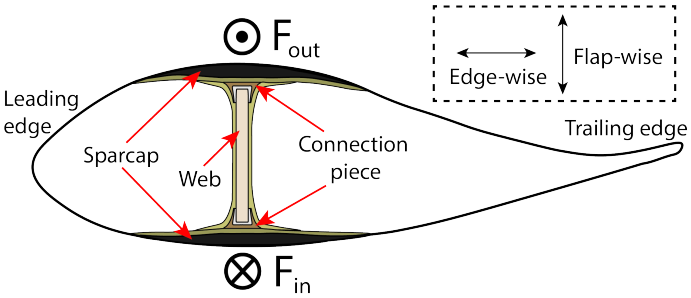

Fig. 1 Wind turbine blade cross-section with the flap-wise bending represented by the two force arrows F_{out} and F_{in}. The primary structural components for flap-wise bending are marked by the arrows from the designations.

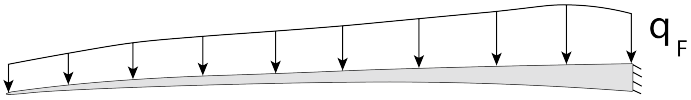

Fig. 2 Line force causing flap-wise bending on the wind turbine blade looking at the leading edge.

Siemens Gamesa Renewable Energy [SGRE] [1] utilises a unique manufacturing method to produce the wind turbine blades, where the laminates in the connection are infused with resin simultaneously with the rest of the blade, which limits potential solutions.

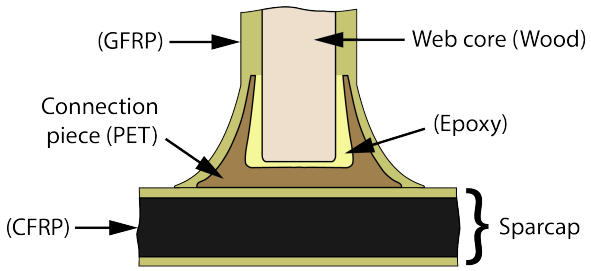

Fig. 3 Currently used concept for web to sparcap connection. Materials are enclosed in parentheses.

In the present study a simplified model for stress analysis was developed, and factor of safety [FoS] calculated using maximum-stress and Puck failure criteria. This model was used in a sequential quadratic programming optimisation to reach an optimised design, which was further improved upon using synthesis based on analyses of the models, optimisation and results.

This paper presents a new design of the connection piece with results from the applied analyses. The new design is derived from the presented methodology for improving the connection between web and sparcaps, which can be used at SGRE [1] for larger wind turbine blades.

2 Method

The connection area is innovated upon to create new connection concepts, that will be optimised to create a new design for the connection. The structural optimisation of the new concept is based upon restrictions on mechanical properties such as weight, stiffness and volume of epoxy pockets of the current concept, while maximising the lowest FoS for various failure criteria. This requires analyses of the mechanical properties of the current connection, which the new concept must improve upon. The optimised solution will be further analysed and improved upon to reach a final design, which is compared to the current solution. The methods and analyses used to obtain the final design for the connection piece are outlined in figure 4.

2.1 Concept Generation

The new concept consists of the same materials as the current solution. To formulate engineering parameters for selection of the best design, the Quality Function Deployment [QFD] method [4] is used. With the QFD method, general wishes and requirements are transformed into specific engineering parameters with a relative importance, which is used to identify the FoS as the objective of the optimisation. To ensure an improved solution is found, other engineering parameters are selected as constraints.

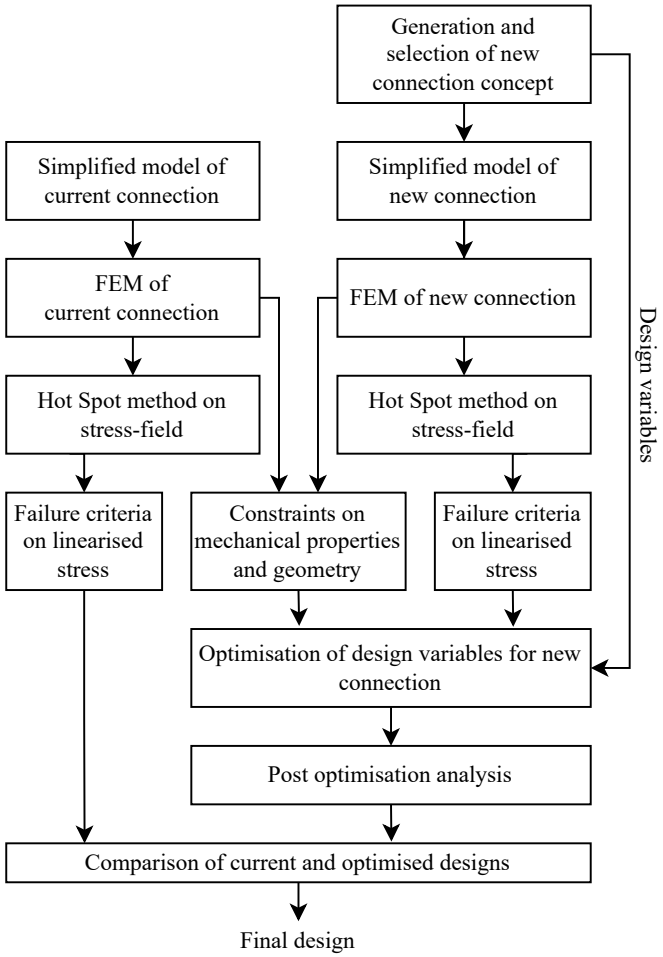

Fig. 4 Work flow for modelling, analysing and improving the connection. The simplified model and FEM of the current connection outputs the structural requirements used as constraints and for comparison with the new design.

The generation of concepts is based on a morphological analysis [4]. The analysis included splitting the load on the connection piece into the different in-plane load components displayed in figure 5, and developing concepts for each. Brainwriting was used as the idea generation method to form solutions to each of the in-plane loads, which were then combined to form concepts. Hereafter, a concept was selected based on the fulfillment of the engineering parameters. This was aided by the use of a weighted evaluation matrix, to indicate relative strengths and weaknesses in terms of the engineering parameters for the different concepts.

In order to build a model of the new concept, the required parameters to describe the concept are determined. For the optimisation, a set of design variables are chosen from these parameters.

2.2 Simplified Model

For modelling both the current and new connection concept, a simplified model of the cross-section illustrated in figure 3, with a $1mm$ thickness was utilised.

From the full blade model, work equivalent line loads along the top and bottom of the web were provided by SGRE [1]. The maximum in-plane loads found throughout the length of the blade were used, as these loads are assumed to be critical for the connection. Using static equilibrium, the line loads were moved to the top of the model from the original position depicted in the right part of figure 5, and applied over the simplified model.

The sparcap is partly replaced by a fixed support based on an assumption given: the high stiffness of the CFRP compared to the GFRP, and the large thickness of the sparcap relative to the web. The $1mm$ thick cross-section is modelled with plane strain, as the cross-section is cut out from a more than $100m$ long blade. Plane strain is assumed, to focus analyses on the in-plane loads and keep the geometry in-plane.

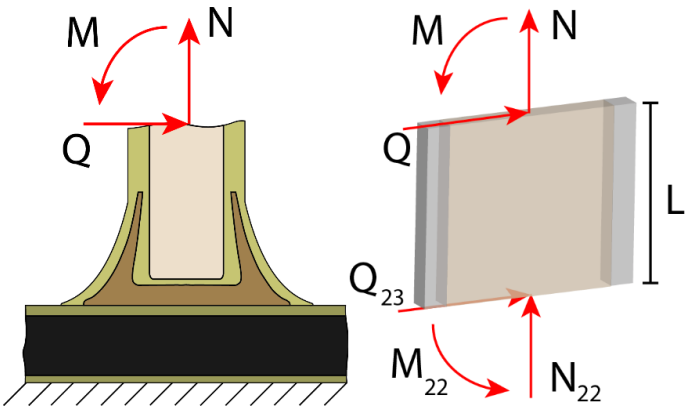

Fig. 5 Simplified model with applied force components, and free body diagram of web used to translate loads with static equilibrium.

2.3 Finite Element Modelling

Finite element modelling [FEM] with static structural analyses of the simplified model described in section 2.2, was utilised to determine the mechanical properties of the current and new designs.

The analyses were geometrically and materially linear, with solid elements for non composite materials and solid shell elements for the composite materials. With the applied maximum in-plane loads, the displacement and thereby stress-fields are obtained and analysed. Due to the transitions between materials with different stiffness, free or sharp edges, stress singularities are present in the stress-field. A singularity at the sharp edge is shown at the point of maximum stress in figure 6. Singularities are handled in section 2.4.

Fig. 6 Shear stress-field in MPa in the connection piece.

2.4 Hot Spot

The stresses in the stress singularities were approximated using the Hot Spot method [5]. The approximated stresses were then used in conjunction with the failure criteria to estimate the FoS. The Hot Spot method is used to investigate a critical point in a structure due to a discontinuity or notch. The method is built into ANSYS [6] with stress linearisation along a given path. The stress-field is separated into a membrane σ_m, bending σ_b and non-linear peak σ_{nlp} stress part. This is exemplified with a Bernoulli-Euler beam in figure 7. The linearised and evaluated stress are described by equation 1 and 2 respectively.

$$S_{Lin} = \sigma_m + \sigma_b \tag{1}$$

$$S_{Ev} = \sigma_m + \sigma_b + \sigma_{nlp} \tag{2}$$

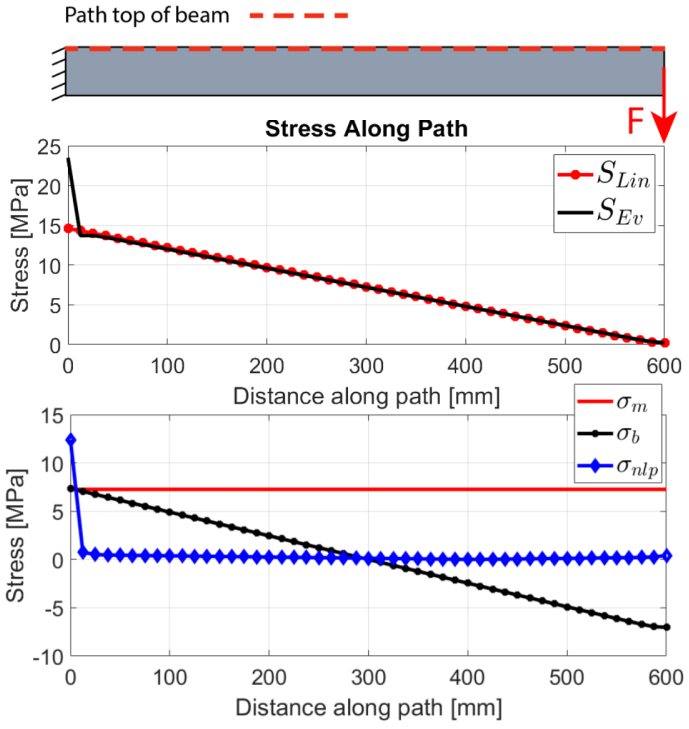

Fig. 7 Figure and graph of the Bernoulli-Euler beam with both the membrane, bending, non-linear peak, linearised and evaluated stress along the shown path.

The Hot Spot method is primarily used through the thickness of the laminates to filter the stress singularities at the interface between laminate and connection piece. The method is most effective if the stresses are linear along the path towards the singularity. Through the thickness of a laminate, first order shear deformation theory which is used in the solid shell elements in ANSYS, predicts piece-wise linear stresses dependent on the orientation of the laminae. When the laminate uses $\pm 45°$ orientations of laminae, as used on the web and connection, the stress will be piece-wise linear with the same gradient in all elements apart from the element at the stress singularity. Based on this the Hot Spot method is considered reasonably accurate at approximating the stresses for use in the optimisation.

2.5 Failure Criteria

To determine the strength of the connection, several failure criteria are used on the stress-field to calculate FoS for the GFRP and connection piece. The failure criteria are split into the orthotropic strengths [7] of the connection piece and Puck [8] failure criterion of the GFRP.

The connection is evaluated in a plane, where the PET foam has the same strength in all directions, which means the strength is only divided into tension, compression and shear. These individual strengths are used on the stress fields to predict failure, as the Von Mises stress cannot be used on orthotropic materials [7]. The FoS in tension and compression is evaluated as the maximum and minimum principal stresses, compared to the strength in the respective directions, as stated in equation 3 and 4. The shear FoS is evaluated by comparing the maximum shear stress to the shear strength, as stated in equation 5.

$$SF_t = \frac{\max\{\sigma_p\}}{S_t} \tag{3}$$

$$SF_c = \frac{\min\{\sigma_p\}}{S_c} \tag{4}$$

$$SF_s = \frac{\max\{|\tau_{xy}|\}}{S_s} \tag{5}$$

SF_t, SF_c and SF_s is the FoS in tension, compression and shear respectively, while σ_p denotes the principal stresses and τ_{xy} the shear stress. S_t, S_c and S_s is the strength in tension, compression and shear respectively.

On the composite material, the 2D Puck failure criterion is used to predict failure, given the plane strain and in-plane loading. The Puck failure criterion treats fibre and matrix failure separately [8], with fibre failure SF_F being treated as stated in equation 6 and matrix failure SF_M as in figure 8, with the equation for mode A, B and C stated in equation 7, 9 and 11 respectively.

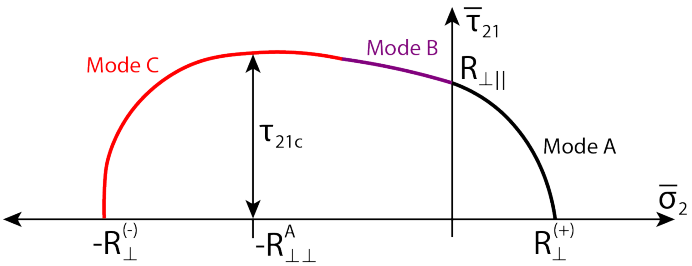

Fig. 8 Puck failure criteria for matrix failure. Stresses outside the curve cause failure. The nomenclature is listed in table 1.

$$SF_F = \frac{\sigma_1}{R_{\|}^{(+)}} \textbf{ or } \frac{\sigma_1}{-R_{\|}^{(-)}} \tag{6}$$

$$SF_M = \sqrt{\left(\left(\frac{1}{R_{\perp}^{(+)}} - \frac{p_{\perp\|}^{(+)}}{R_{\perp\|}}\right)\sigma_2\right)^2 + \left(\frac{\tau_{21}}{R_{\perp\|}}\right)^2} + \frac{p_{\perp\|}^{(+)}}{R_{\perp\|}}\sigma_2 \tag{7}$$

for $\sigma_2 \geq 0$ (8)

$$= \sqrt{\left(\frac{\tau_{21}}{R_{\perp\|}}\right)^2 + \left(\frac{p_{\perp\|}^{(-)}}{R_{\perp\|}}\sigma_2\right)^2} + \frac{p_{\perp\|}^{(-)}}{R_{\perp\|}}\sigma_2 \tag{9}$$

for $\sigma_2 < 0$ **and** $\left|\frac{\sigma_2}{\tau_{21}}\right| \leq \left|\frac{R_{\perp\perp}^{A}}{\tau_{21c}}\right|$ (10)

$$= \left(\left(\frac{\tau_{21}}{2(1+p_{\perp\perp}^{(-)})R_{\perp\|}}\right)^2 + \left(\frac{\sigma_2}{R_{\perp}^{(-)}}\right)^2\right)\frac{R_{\perp}^{(-)}}{-\sigma_2} \tag{11}$$

for $\sigma_2 < 0$ **and** $\left|\frac{\sigma_2}{\tau_{21}}\right| \geq \left|\frac{R_{\perp\perp}^{A}}{\tau_{21c}}\right|$ (12)

Description	Puck Notation
Fibre tensile strength	$R_{\|}^{(+)}$
Fibre compression strength	$R_{\|}^{(-)}$
Matrix tensile strength	$R_{\perp}^{(+)}$
Matrix compression strength	$R_{\perp}^{(-)}$
In-plane shear strength	$R_{\perp\|}$
Strength at fracture plane	$R_{\perp\perp}^{A}$
Stress in fiber direction	σ_1
Stress in tranverse direction	σ_2
In-plane shear	τ_{21}
Maximum value of τ_{21}	τ_{21c}
Inclination parameters	p

Tab. 1 Nomenclature used for the Puck failure criterion [8].

2.6 Optimisation

Optimisation is used to maximise the lowest FoS from the failure criteria in the connection expressed in equation 13, which is the objective function.

$$SF = \mathbf{min}(SF_c, SF_t, SF_s, SF_{puck}) \tag{13}$$

The objective function outputs the smallest entry in an array of FoS and is thereby non-differentiable, given a different entry in the array can become the smallest at certain points. In points where the lowest FoS changes between different failure criteria, a discontinuity will be present in the gradient of the objective function. This is a problem, as the gradient is needed in gradient based optimisation methods and for evaluating optimality conditions. Using finite difference approximations for the gradient effectively applies a filter to the gradient. As such changes and discontinuities in the gradient within each step is smoothed, and a gradient can be approximated in the discontinuity. It is already necessary to use finite difference approximations of the gradient, since the evaluation of the FoS in a point does not include the gradient with respect to the design variables. The objective function will be used as if it is continuous and differentiable, while using the optimisation scheme Non-linear Programming by Quadratic Lagrangian [NLPQL], described in [9].

The method optimises the objective function with several constraints based on the mechanical properties of the current connection stated in equation 14 to 16, and certain geometrical requirements. The stiffness constraint is handled by using the same loads and having a smaller displacement in a given point, as stated in equation 15.

$$g_m(\vec{x}) - m_c \leq 0 \tag{14}$$
$$g_d(\vec{x}) - d_c \leq 0 \tag{15}$$
$$g_{pv}(\vec{x}) - V_{pc} \leq 0 \tag{16}$$

g_m, g_d and g_{pv} denotes the mass, displacement and resin pocket volume respectively, and is evaluated using FEM. m_c, d_c and V_{pc} are the mass, displacement and resin pocket volume of the current solution. $\vec{x}$ is the vector of design variables listed in table 2.

The NLPQL method [9] consists of the Lagrange function in equation 17, with the Lagrange multipliers λ, the objective function $f = -SF$, constraint equations g and number of constraint equations n.

$$L(\vec{x}, \vec{\lambda}) = f(\vec{x}) - \sum_{i=1}^{n} \lambda_i g_i(\vec{x}) \tag{17}$$

The non-linearity in the objective and the constraints are handled by forming a subproblem, which is formed by linearisation of the constraints and applying a quadratic approximation to the Lagrangian function. This yields the subproblem stated in equation 18 and 19 where: $\vec{d}$ denotes the direction to change the design variables, B is a positive definite approximation of the Hessian by the Broyden-Fletcher-Goldfarb-Shanno [BFGS] method [10] and k denotes the current iteration. Optimum is found by sequentially solving the subproblem from a set of initial values for the design variables [9].

$$\mathbf{Minimise}: \quad \frac{1}{2}\vec{d_k}^T \mathbf{B}_k \vec{d_k} + \nabla f(\vec{x})^T \vec{d_k} \tag{18}$$
$$\mathbf{Subject\ to}: \quad \nabla g_i(\vec{x})^T \vec{d_k} + g_i(\vec{x}) \leq 0 \tag{19}$$

This quadratic subproblem is solved for the direction of change, which is used as the direction for a line search. The step size α_k is determined and the next iteration of design variables is found by equation 20.

$$\vec{x}_{k+1} = \vec{x}_k + \alpha_k \vec{d_k} \tag{20}$$

By using the gradient as a convergence criteria in the NLPQL algorithm, the first order necessary optimality condition stated in equation 21 will be fulfilled to the desired degree.

$$\nabla f = 0 \tag{21}$$

The second order optimality condition requires that the Hessian must be positive definite. The Hessian is used to differentiate between local maximum, minimum and inflection points. The use of the BFGS formula, ensures a positive definite approximation to the Hessian, which implies that the method will always converge to a local minimum. As such the second order optimality condition is upheld [10].

2.7 Post Optimisation Analysis

The resulting design is further improved upon and partially validated with analysis on the design and changes to the design variables or other parts of the design. Any changes to the design based on the post optimisation analyses subsequently undergoes the validating analyses from this section.

The analysis of structural failure shows the critical parts of the optimised structure. This is used to identify new stress singularities and evaluate the influence of parameters on the FoS. By altering the parameters to increase complexity in the most critical parts, further improvement on the FoS can be achieved. To avoid increase in the computational cost, simplifications in the less critical parts can be made. This improves the efficiency and potential of the optimisation, as the chosen design variables will have greater influence on the FoS.

After the optimisation, the values of the design variables have too many decimals for manufacturing purposes. Therefore, the design variables are rounded off to the closest integer value in appropriate units. Due to the computational cost of the models, the optimisation is likely to stop by reaching the limit on iterations rather than the optimality condition. A dominating stress singularity unaccounted for with the Hot Spot method could also cause the wrong FoS to be the lowest. In these cases,

the gradient ∇SF determines, which of the integer values the design variable is rounded to.

A rotation and vertical movement of the web core relative to the sparcap lowers the FoS. Therefore, the current connection and the optimised design are analysed with a rotated web core. The normal and shear forces are applied parallel and perpendicular to the rotated web respectively, however the forces do not follow the web during deformation in the structural analysis.

The constraints that are upheld during the optimisation are investigated to see if changes to the constraints have a large influence. To reduce the number of additional optimisations the influence of the mass is investigated based on the expected correlation with the FoS.

The NLPQL optimisation scheme converges to local minima [9]. To account for the possibility of additional local minima and increase the chance of finding the global minimum, the optimisation is started from different initial points, which are chosen as different plausible solutions.

3 Results

3.1 New Concept

In the selected new concept the connection piece is split into two pieces, which is illustrated in figure 9. The idea of the concept is to more effectively allow the rotational tolerance with less epoxy pocket volume. Given the higher density of epoxy relative to the PET foam of the connection piece, a reduction in epoxy can allow more mass in the connection piece to achieve a stronger geometry.

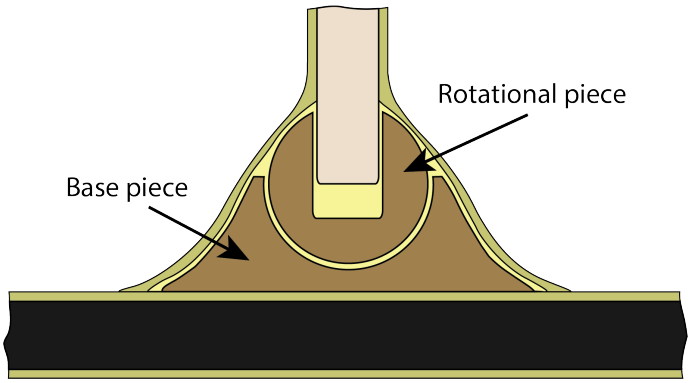

Fig. 9 The selected concept with the connection piece divided into a base and a rotational piece.

The selected concept has been parameterised to choose the design variables, which the optimisation changes. The constant parameters and design variables are stated in figure 10 and listed in table 2.

Constant Parameters	Design Variables
x_3	x_1
l_1	x_2
δ_r	y_2
y_1	y_3
	L_1
	L_2

Tab. 2 Geometrical parameters used to describe the selected concept.

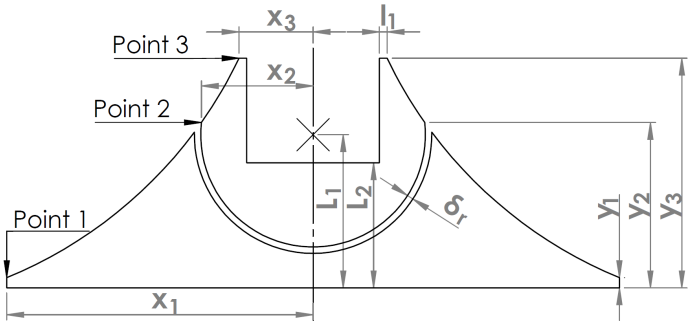

Fig. 10 Parameters used to describe the new concept. The outer curves are defined by a circular arc through point 1, 2 and 3 to reduce the number of parameters necessary. The inner curve is defined by a circle with centre at (0, L1) and radius from the centre to Point 2.

3.2 Optimisation of New Concept

The optimisation of the initial values of the design variables yielded the optimised values, both are stated in table 3.

DV	y_2	y_3	x_1	x_2	L_1	L_2
ID	35.00	50.00	65.00	25.00	35.00	25.00
OD	27.82	54.49	45.24	26.49	33.15	15.21

Tab. 3 Initial and optimised values in mm of the design variables. DV, ID and OD are the design variables, initial design and optimised design respectively.

	Current	Initial	Optimised
Lowest FoS	0.8863	1.258	1.844
Lowest FoS relative to current	100%	142%	208%
Deformation $[mm]$	1.112	1.071	0.9684
Mass $[g]$	1.379	1.528	1.267
Epoxy volume $[mm^3]$	739.4	536.2	573.5
Allowable rotation limit $[^\circ]$	14	> 14	> 14
Allowable vertical movement limit $[mm]$	30	< 30	> 30

Tab. 4 Resulting values of objective and constraints. The limit on allowable rotation and vertical movement is set by an allowed decrease in FoS, which is not determined. Therefore, the new designs are listed as above or below the current limits based on the geometrical clearance.

The analyses used to evaluate the objective function and constraint functions yielded comparable results, which are shown in table 4. The table states that the new design has a higher FoS in the connection. The initial design had more mass, however after the optimisation, the mass constraint was upheld while the strength also increased. In table 4 the lowest FoS for each of the designs are stated, where the lowest FoS was given from SF_s on the connection piece for the current solution, and SF_{puck} for the optimised solution on the GFRP.

3.3 Post Optimisation Analysis

During the optimisation, several simplifications were made to achieve computational efficiency. The optimised design was therefore analysed more thoroughly with the methods in section 2.7.

3.3.1 Failure Mode

The analysis of the failure mode showed failure in the GFRP, which was caused by a stress singularity. Applying the Hot Spot method on this stress singularity and mesh refinement yielded the changes to the FoS, stated in table 5.

	Optimised	Post processed
Puck FoS	1.844	2.406
Shear FoS	1.851	1.858
Principal FoS	4.304	4.318
Lowest FoS relative to current solution	208%	210%

Tab. 5 Results of the optimised design before and after post processing.

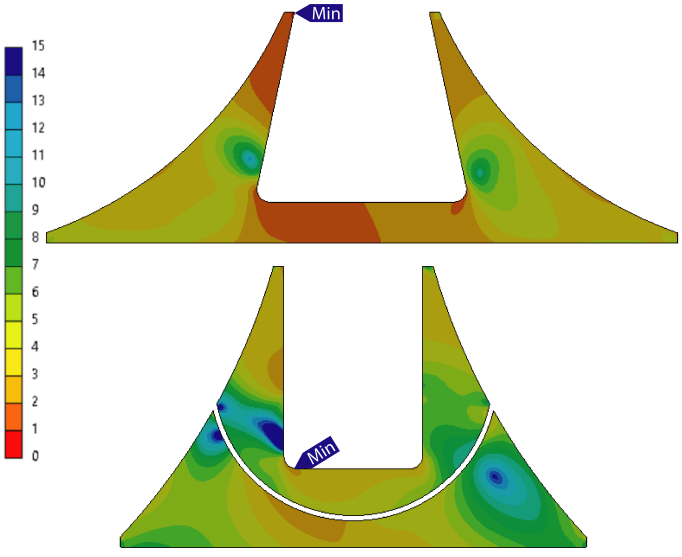

Fig. 11 Shear FoS for current and optimised design.

The lowest FoS changed from the Puck criterion on the GFRP to the shear strength on the connection piece. Given the lowest FoS is found in the inner fillet, which is shown with the shear FoS plot in figure 11 for the current and optimised designs, this was chosen as an improvement area.

In order to investigate the inner fillet, the web core end and the hole in the rotational piece were turned into half-circles. This yielded the design shown in figure 12 with the FoS listed in table 6.

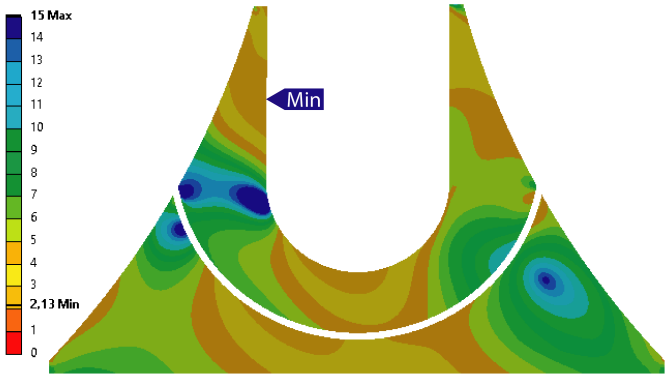

Fig. 12 Shear FoS with circular web.

	Square web	Circular web
Puck FoS	2.41	2.30
Shear FoS	1.86	2.13
Principal FoS	4.32	8.18
Lowest FoS relative to current solution	210%	240%

Tab. 6 FoS for the original and changed web designs.

The circular web is not investigated further since it is not considered a viable solution due to manufacturing considerations following the discussion in section 4.1.

3.3.2 Rounding of Dimensions

The gradient in the last point of the optimisation stated in table 7 with regards to the FoS, is used to manually adjust the design variables in order to improve the FoS. Due to the change in failure mode, the gradient is calculated with respect to the shear FoS.

	$\frac{\partial SF}{\partial y_2}$	$\frac{\partial SF}{\partial y_3}$	$\frac{\partial SF}{\partial x_1}$	$\frac{\partial SF}{\partial x_2}$	$\frac{\partial SF}{\partial L_1}$	$\frac{\partial SF}{\partial L_2}$
c_{SF} $\left[\frac{1}{mm}\right]$	-0.049	0.040	0.078	-0.198	0.011	-0.034

Tab. 7 Gradient c_{SF} approximated by central difference for shear FoS with respect to design variables.

The resulting dimensions rounded in the direction of the gradient, and FoS can be seen in table 8 and 9 respectively with the optimised design.

DV	y_2	y_3	x_1	x_2	L_1	L_2
OD	27.82	54.49	45.24	26.49	33.15	15.21
MCD	27	55	46	26	34	15

Tab. 8 Optimised and manually changed values in mm of the design variables. MCD is the manually changed design.

	MCD	Comparison
Puck FoS	2.100	87.3%
Shear FoS	1.915	103%
Principal FoS	6.005	139%
Lowest FoS relative to current solution	216%	103%

Tab. 9 FoS for the optimised design before and after manually rounding based on gradients.

3.3.3 Rotated Web

The web is rotated $14°$ in order to evaluate the FoS at the allowable rotation limit. On the connection components, the shear FoS was the lowest for the existing and new optimised design in the inner fillet for the web cutout, shown in figure 13.

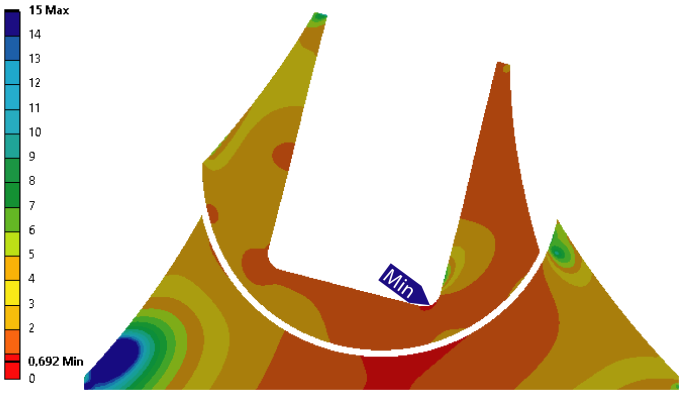

Fig. 13 Shear FoS plotted on rotated connection piece.

The FoS for the current and new optimised solution is stated in table 10.

	Current	New optimised
Puck FoS	0.728	1.04
Shear FoS	0.385	0.692
Principal FoS	0.526	1.33
Lowest FoS relative to current solution	100%	180%

Tab. 10 FoS for the current and new designs with a web rotated to the tolerance of the existing design.

3.3.4 Mass Considerations

The optimisation procedure was run with the mass constraint changed to $\pm 10\%$, which yielded the values of the design variables stated in table 11. The optimisations with different mass constraints were run with a different initial design point.

	y_2	y_3	x_1	x_2	L_1	L_2	Mass	FoS
ID2	18.0	48.0	46.0	30.0	51.0	10.0	1.14	1.58
-10%	18.3	50.1	41.7	29.1	51.3	11.8	1.14	1.77
$+10\%$	19.5	54.0	38.8	28.3	58.8	16.2	1.18	1.94

Tab. 11 Initial and optimised values of the design variables in mm, mass in g and FoS with the mass constraint changed to $\pm 10\%$ of the current connection. ID2 is the initial design.

From the different starting point used, a new local minima was found for both the $+$ and -10% cases. The local minima in the $+10\%$ case was an improvement compared to the optimised design listed in table 4, in terms of both FoS and mass. Therefore, the design is chosen as the final design and put through the analyses of section 2.7 again, except for the rotation of the web core, since the results were unchanged in the analysis of the first optimised design.

3.4 Final Design

After the post-processing of the new local minima, the final design shown in figure 14, was achieved, with the design values expressed in table 12.

Dimensions	y_2	y_3	x_1	x_2	L_1	L_2
Final design $[mm]$	19	55	38	28	52	16

Tab. 12 The final set of design variables.

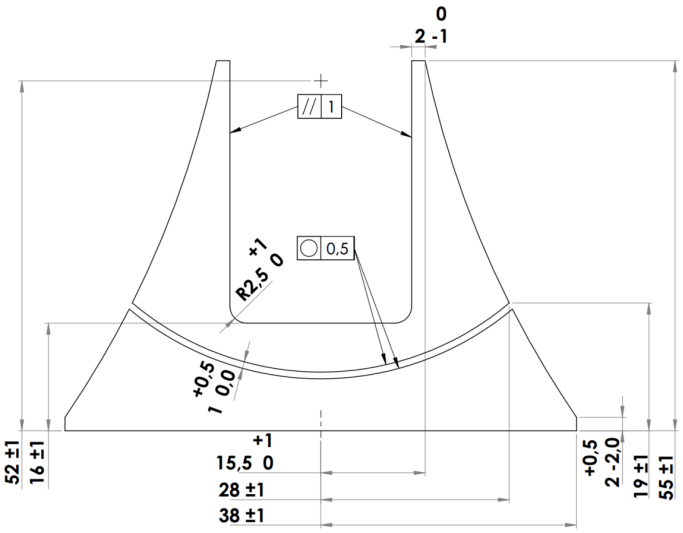

Fig. 14 Blueprint of final design with dimensions in mm.

The final design evaluated with respect to the other mechanical properties, and compared with the current solution are stated in table 13.

	Final	Relative to current
Lowest FoS	2.02	228%
Create and maintain structural connection	√	√
Remain within area of modelling	√	√
Keep web and sparcap unchanged	√	√
Mass of PET foam and resin pockets $[g]$	1.173	85.1%
Displacement of point related to stiffness $[mm]$	1.00	90.1%
Volume of resin pockets $[mm^3]$	574.6	77.7%
Allowable rotation limit [°]	>14	>100%
Allowable vertical movement limit $[mm]$	>30	>100%

Tab. 13 Mechanical properties for final design and comparison with the existing design. The lowest FoS is with respect to shear.

3.4.1 Validity of Puck Failure Criterion

For validation of the 2D Puck failure criterion, additional failure criteria from [7] were used. This yielded the results listed in table 14.

	Final design
Puck 2D FoS	2.39
Puck 3D FoS	2.39
Tsai-Wu 2D FoS	2.64
Tsai-Wu 3D FoS	2.59

Tab. 14 Evaluated failure criteria for final design.

4 Discussion

The evaluation of the stress-field following the methodology described in section 2, is purposely oversimplified. This is done to have a computationally efficient model for use in the optimisation, and speed up the process of improving the connection. However, the efficiency comes at a cost of modelling accuracy. Due to the simplifications, the results for the FoS are subject to uncertainties. Therefore, experiments or more accurate models including non-linear behavior or fracture mechanics should be applied to validate the FoS.

4.1 Optimisation

Following the methodology of analysing the failure mode, the presence of a stress singularity was shown to affect the FoS for the Puck failure criterion. Applying the Hot Spot method to the stress singularity increased the FoS and changed the failure mode to shear. As the optimisation used the lowest FoS, it reached a point where the Puck and shear FoS were similar. If the stress singularity were taken into account before the optimisation procedure, it could have optimised more with regards to shear and reached a higher FoS. A better optimisation scheme can be achieved by removing the effect of singularities as the optimisation progressed.

Furthermore, the optimisation was bound by the chosen parameterisation and constraints. Table 3 shows that the optimisation scheme lowered all dimensions except y_3 and x_2. This is due to the mass of the initial connection piece being higher than the maximum allowable mass, as stated in table 4. During the optimisation, the design was changed to lower the mass to uphold the constraint while increasing the FoS. However, the investigation of the mass constraint with the results in table 11, indicated that the mass constraint has no clear connection to the FoS. This is seen by the FoS being increased without an increase in mass, which contradicts the expected relation of more mass providing more strength. The lack of correlation between mass and strength could be explained by having a different constraint limiting the FoS. It could also be explained by a different failure mode which is unaffected by the chosen design variables. Analysing the Lagrange multipliers from the optimisation would show which constraints are active and limiting further improvement, if any [10].

The analysis of the failure mode and rotational web core tolerance, indicated that failure occur at the inner fillet. This location seemed less affected by the design variables and was analysed by changing the inner fillet, which increased the FoS, as shown in table 6. This indicates the possibility of further improvement by including parameters regarding the inner groove geometry in the design variables. However, changing the web core end and making the inner fillet a design variable, would increase the time for the optimisation. Furthermore, it is assessed that changing the web core end is not a viable solution given the extra manufacturing needed.

With more than one local minima present as shown in section 3.3.4, it could be beneficial to analyse the solution space more thoroughly. This is due to the possibility of finding improved designs with a higher FoS. Analyses intended to find the global minimum have a high computational cost. However, simple methods such as including additional initial design points or modelling of the response surface, could be used to increase the probability of finding improved local minima [10].

4.2 Final Design

The additional failure criteria applied to the final design showed an increase in FoS, with the use of the Tsai-Wu criteria shown in table 14. The 3D version of the Puck and Tsai-Wu criteria was used to take the strength through the thickness of the laminates into account, as the assumption of plane stress in a laminate is not necessarily valid for curved laminates. However, table 14 shows that the difference between the 2D and 3D criteria was negligible at less than 1% in case of the Puck criterion. The used failure criterion is therefore considered valid, and uncertainties

towards the FoS are expected to emanate from the evaluation of the stress-field.

In order to manufacture the final design, tolerances and manufacturing procedures have to be considered on the design in figure 14. The tolerances are standardised to $\pm 1mm$ in most cases. However, some of the tolerances e.g. on the inner fillet, are based on structural considerations. For the inner fillet the tolerance is given as $+1/0mm$ to ensure that the fillet is only allowed to increase in size. This was shown in the analysis of the parameterisation to increase the FoS, while still allowing for placement of the web core end.

5 Conclusion

The methodology of the structural optimisation applied yielded a final design, which has a safety factor of 228% compared to the current solution, while upholding other mechanical constraints. This included a decrease in mass and volume of resin pockets by 14.9% and 22.3% respectively, and an increase in the stiffness by 11% compared to the current solution. The methodology and the final design can be used at SGRE [1], for future development of larger blades.

Through further analysis of the design space, additional local minima may be found, which could have a higher FoS. A better parameterisation of the design could also lead to improvements, as some stress concentrations were unaffected by the design variables.

The authors consider the methodology useful for the structural optimisation of the web to sparcap connection, since it is inferred that a stronger design has been achieved based on the models used. However, further validation of the final design using experiments or more advanced models, is needed as an extension of the methodology.

Acknowledgement
The authors of this work gratefully acknowledge Grundfos for sponsoring the 10th MechMan symposium.

Furthermore, we acknowledge Réne Sørensen and Anders Libak Strandbygaard from Siemens, for providing data and knowledge about the wind turbine blades produced at Siemens Gamesa Renewable Energy.

References

[1] S. G. R. Energy, "Offshore Blade Structural Design Team at Siemens Gamesa Renewable Energy," 2022. Assensvej 11, 9220 Aalborg.

[2] United Nations Environment Programme, "Goal 7: Affordable and clean energy," 2022. https://www.unep.org/explore-topics/sustainable-development-goals/why-do-sustainable-development-goals-matter/goal-7.

[3] Gurit, "*Gurit wind energy handbook*," in 2 Aerodynamics, Gurit, 2022. https://www.gurit.com/.

[4] D. G. Ullman, *The mechanical design process*. McGraw-Hill Higher Educatio, sixth ed., 2018.

[5] E. Neime, *Stress determination for fatigue analysis of welded components*. Woodhead Publishing, first ed., 1995.

[6] ANSYS, "POST1 - Stress Linearization," 2022. https://www.mm.bme.hu/~gyebro/files/ans_help_v182/ans_thry/thy_post4.html.

[7] R. M. Jones, *Mechanics of composite materials*. Taylor and Francis Group, second ed., 1999. pp. 102-120.

[8] A. Puck and H. M. Deuschle, "Progress in the puck failure theory for fibre reinforced composites : Analytical solutions for 3d-stress," *Composites science and technology*, vol. 62, no. 3, pp. 371–378, 2002.

[9] K. Schittkowski, "Nlpql: A fortran subroutine solving constrained nonlinear programming problems," *Annals of operations research*, vol. 5, p. 500, 1985.

[10] J. Nocedal and S. J. Wright, *Numerical optimization*. Springer, second ed., 2006. pp. 135-143, http://www.apmath.spbu.ru/cnsa/pdf/monograf/Numerical_Optimization2006.pdf.